GEOPHYSICS, VOL. 48, NO. 6 (JUNE 1983); P. 754–774, 16 FIGS.

Werner deconvolution for automated magnetic interpretation and its refinement using Marquardt's inverse modeling

Chao C. Ku* and John A. Sharp*

ABSTRACT

We present a deconvolution for automated magnetic interpretation based on Werner's (1953) simplified thin-dike assumption which leads to the linearization of complex nonlinear magnetic problems. The usefulness of the method is expanded by the fact that the horizontal gradient of the total field caused by the edge of a thick interface body is equivalent to the total field from a thin dike. Statistical decision, numerical iteration, and a seven-point operator are used to improve approximations of susceptibility, dip, depth, and horizontal location of the source. Marquardt's nonlinear least-squares method for inverse modeling is then used to refine automatically the first approximation provided by the deconvolution. Synthetic and real total-field data are used to demonstrate the process.

INTRODUCTION

This paper first deals with a deconvolution for automated magnetic interpretation originally pioneered by Werner (1953), and then with a further refinement of the Werner interpretation using Marquardt's nonlinear least-squares best fit as an approach to inverse modeling.

The Werner deconvolution method has been used by some geophysicists since 1968 as part of a routine automated magnetic interpretation system. The results of applying this method were first published by Hartman et al (1971). Jain (1976) published an article on Werner deconvolution using model studies. Recently, Stanley (1977) presented a manual interpretation procedure based on the thin dike and interface relationship.

Thus application of the Werner deconvolution is now well known. The purposes of this paper are in essence, to review some fundamentals of the method, to show its statistical nature, and to show the necessity for using iteration for reducing and eliminating interferences and for improving its degree of approximation. We use real field data as well as synthetic models of various geometrical configurations for our discussions.

It will be shown that just as the Werner total-field solution is a good indicator of a thin-dike body, so is the Werner horizontal-gradient solution a good indicator of the edge of a thick interface body. Intelligent use of these two extreme types of solutions can lead to a close approximation both in terms of depth estimation and its ability to reveal the geometry of different magnetic bodies including those which may lie somewhere between a thin dike and the edge of a thick interface. Indeed, with some experience one can arrive at a very good interpretation directly using Werner's depth, horizontal location, dip angle, and magnetic susceptibiilty contrast.

Since it is a close approximation, the Werner solution can further be used as an initial estimate for more refined inverse techniques such as Marquardt's (Johnson, 1969; McGrath and Hood, 1973; Hjelt, 1973; Ku, 1976) to enhance and expand our capability for unravelling geologic structures which might otherwise be less obvious or less certain to the interpreters.

BASIC CONCEPT IN WERNER DECONVOLUTION

The original Werner deconvolution was designed to solve the thin-dike problem. It was Hartman et al (1971) who ingeniously extended the idea by considering the thin-dike body as an approximation in resolving other kinds of magnetic anomalies. Although the consideration appears to be oversimplified, the method does provide a surprisingly wide range of applications in various magnetic situations.

First, let us consider the magnetic anomalies due to a two-dimensional (2-D) vertical thin dike. We choose the x-axis perpendicular to the strike of the dike, the y-axis parallel to the strike, and the z-axis vertical (Figure 1). The dike is extended to infinity in both the y and z directions. The vertical, horizontal, and total magnetic anomalies caused by the dike can then be computed by the following equations (Talwani and Heirtzler, 1964):

$$\mathrm{VMAG}(x, z) = 2 \int\int \left[J_x \frac{2(x' - x)(z' - z)}{R^4} + J_z \frac{2(z' - z)^2 - R^2}{R^4} \right] dx'\, dz', \quad (1)$$

$$\mathrm{HMAG}(x, z) = 2 \int\int \left[J_x \frac{2(x' - x)^2 - R^2}{R^4} + J_z \frac{2(x' - x)(z' - z)}{R^4} \right] dx'\, dz', \quad (2)$$

Presented at the 48th Annual International SEG Meeting November 1, 1978 in San Francisco. Manuscript received by the Editor November 19, 1979; revised manuscript received November 11, 1982.

*Formerly Aero Service Division, Western Geophysical Company of America, Houston, TX; presently Amoco Production Company, P.O. Box 3092, Houston, TX 77001.

and

$$\mathrm{TMAG}(x, z) = \mathrm{HMAG}(x, z)\cos I \sin\alpha + \mathrm{VMAG}(x, z)\sin I, \tag{3}$$

where

I = magnetic inclination of the main field $\mathbf{F}$,
α = strike of the dike as measured from magnetic north, positive counterclockwise,
$R^2 = (x' - x)^2 + (z' - z)^2$,
$\mathbf{J} = (J_x, J_z)$ = polarization vector = induced + remanent magnetization.

Let D be the depth to the top of the dike, and $2\Delta T$ the thickness of the dike (Figure 1). When ΔT is small compared to depth D, ($\Delta T \ll D$), namely, the dike is thin as viewed from the point of observation at $P(x, 0)$, then a straightforward integration of equations (1) and (2) leads to the following simple but useful approximations:

$$\mathrm{VMAG}(x, z) = 2\int_D^\infty \int_{-\Delta T}^{\Delta T} \left[J_x \frac{2(x' - x)(z' - z)}{R^4} + J_z \frac{2(z' - z)^2 - R^2}{R^4} \right] dx'\, dz',$$

$$\mathrm{VMAG}(x, 0) \cong 2 \cdot 2\Delta T \left(J_x \int_D^\infty \frac{-2xz'}{R^4}\, dz' + J_z \int_D^\infty \frac{2z'^2 - R^2}{R^4}\, dz' \right)$$

$$= 2\Delta T \frac{J_z D - J_x x}{x^2 + D^2}; \tag{4}$$

similarly,

$$\mathrm{HMAG}(x, 0) = -2\Delta T \frac{J_x D + J_z x}{x^2 + D^2} \tag{5}$$

and

$$\mathrm{TMAG}(x, 0) = \mathrm{HMAG}(x, 0)\cos I \sin\alpha + \mathrm{VMAG}(x, 0)\sin I = \frac{Ax + BD}{x^2 + D^2}, \tag{6}$$

where

$$A = -2\Delta T(J_x \sin I + J_z \cos I \sin\alpha) \tag{7}$$

and

$$B = 2\Delta T(-J_x \cos I \sin\alpha + J_z \sin I). \tag{8}$$

We can express J_x and J_z in terms of A and B by solving equations (7) and (8). Hence

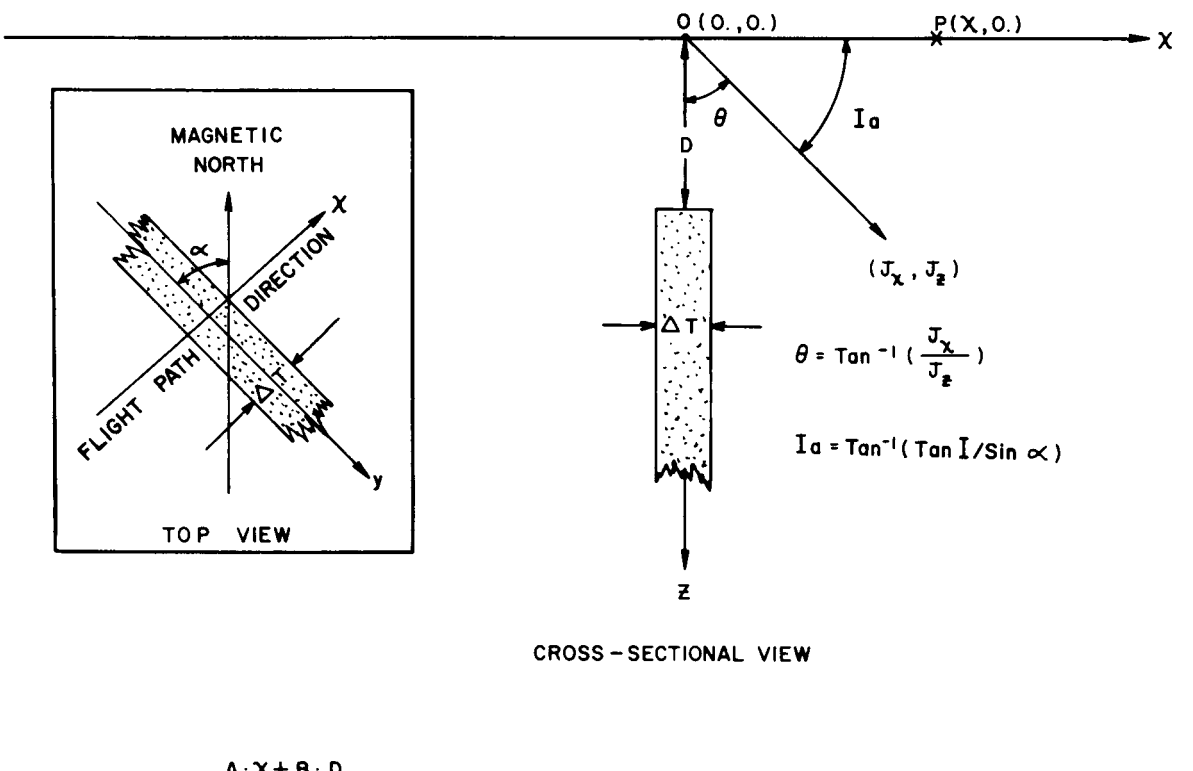

$$\mathrm{TMAG}(X, 0.) = \frac{A \cdot X + B \cdot D}{X^2 + D^2}$$

FIG. 1. Parameters of a 2-D vertical thin dike.

$$J_x = \frac{-BV_x - AV_z}{2\Delta T(V_x^2 - V_z^2)}$$

and

$$J_z = \frac{-AV_x + BV_z}{2\Delta T(V_x^2 + V_z^2)}, \tag{9}$$

where

$$V_x = \cos I \sin \alpha,$$

and

$$V_z = \sin I.$$

Equations (4), (5), and (6) are the basic equations used by Werner in his method of deconvolution for magnetic interpretation. Note that Werner employed a somewhat different approach in his derivations. In fact, the expressions for equations (4) and (5) were also given by Talwani and Heirtzler (1964). The above three equations are obviously identical in mathematical form. Thus for simplicity, we consider equation (6) for total magnetic anomaly only. The results would be the same if we considered equations (4) and (5) for vertical and horizontal magnetic anomalies.

Notice that equation (6) is for the total-field magnetic anomaly when the center of the dike body is located at $(0, D)$. As for an arbitrary horizontal location at (x_0, D), equation (6) should be written

$$\mathrm{TMAG}(x, 0) = \frac{A(x - x_0) + BD}{(x - x_0)^2 + D^2}. \tag{10}$$

By rearranging equation (10), we obtain

$$a_0 + a_1 x + b_0\,\mathrm{TMAG} + b_1 x\,\mathrm{TMAG} = x^2\mathrm{TMAG}, \tag{11}$$

where

$$\begin{aligned} a_0 &= -Ax_0 + BD, \\ a_1 &= A, \\ b_0 &= -x_0^2 - D^2, \end{aligned}$$

and

$$b_1 = 2x_0. \tag{12}$$

If we use an equally spaced four-point Werner operator, arbitrarily choosing the second point of the operator as our reference point, and let

$$\begin{aligned} \mathrm{TM1} &= \mathrm{TMAG}(x - \Delta x, 0), \\ \mathrm{TM2} &= \mathrm{TMAG}(x, 0), \\ \mathrm{TM3} &= \mathrm{TMAG}(x + \Delta x, 0), \end{aligned}$$

and

$$\mathrm{TM4} = \mathrm{TMAG}(x + 2\Delta x, 0),$$

where x is the x-coordinate of the second point and Δx the sample spacing between two consecutive points, then we can write equation (11) in dimensionless simultaneous form as follows:

$$\begin{bmatrix} 1 & -1 & \mathrm{TM1} & -\mathrm{TM1} \\ 1 & 0 & \mathrm{TM2} & 0 \\ 1 & 1 & \mathrm{TM3} & \mathrm{TM3} \\ 1 & 2 & \mathrm{TM4} & 2\mathrm{TM4} \end{bmatrix} \begin{bmatrix} a_0 \\ a_1 \\ b_0 \\ b_1 \end{bmatrix} = \begin{bmatrix} \mathrm{TM1} \\ 0 \\ \mathrm{TM3} \\ 4\mathrm{TM4} \end{bmatrix}. \tag{13}$$

Now, in equation (13) we have four unknowns: a_0, a_1, b_0, and b_1. Thus, in theory if we know the values of TMAG at four appropriate consecutive points, we should be able to obtain the values of these four unknowns simply by solving the simultaneous equation (13) using a simple matrix inversion or by a linear operator as originally proposed by Werner (1953). We can rewrite equation (12) in terms of these four unknowns in the form

$$\begin{aligned} x_0 &= 0.5\, b_1, \\ D &= \sqrt{-b_0 - 0.25\, b_1^2}, \\ A &= a_1, \end{aligned}$$

and

$$B = \frac{1}{D}(a_0 + 0.5\, a_1 b_1). \tag{14}$$

Upon substituting A and B into equation (9), we have for a four-point Werner operator:

$$J_z = \frac{(2a_0 + a_1 b_1)V_z - 2a_1 DV_x}{4\Delta T(V_x^2 + V_z^2)}$$

and

$$J_x = -\frac{(2a_0 + a_1 b_1)V_x + 2a_1 DV_z}{4\Delta T(V_x^2 + V_z^2)}. \tag{15}$$

Finally, we obtain the following results for a thin dike in real physical dimensions in terms of the sample spacing Δx:

$$\text{horizontal position} = 0.5\, b_1 \Delta x + x, \tag{16a}$$

$$\text{depth} = \sqrt{-b_0 - 0.25 b_1^2}\,\Delta x, \tag{16b}$$

$$\text{magnetic susceptibility} = \frac{\sqrt{J_x^2 + J_z^2}}{|\mathbf{F}|}\,\Delta x, \tag{16c}$$

and

$$\text{dip angle} = \tan^{-1}\left(\frac{J_x}{J_z}\right) + I_a. \tag{16d}$$

Let us briefly discuss the physical meaning of equations (16a)–(16d). First, since the value of depth must be real in our physical world, immediately we have the following constraint from equation (16b):

$$-b_0 - 0.25\, b_1^2 > 0. \tag{17}$$

Physically, equation (17) is related to the size of the Werner operator with respect to the size of magnetic anomaly under deconvolution. We should expect intuitively that when the Werner operator is small compared with the anomaly size the operator will see only a small and hence nearly linear portion of the magnetic anomaly. As a result, it would yield a depth solution which is much deeper than the true depth. On the other hand, if the operator is too large, the operator would very likely see multiple peaks from adjacent anomalies, thus resulting in either erroneous calculation or failure to satisfy the constraint of equation (17). In general, the optimum size of the Werner operator should be of the same order of magnitude as the anomaly size such that the operator is small enough to see only a single peak (or trough) yet large enough to cover sufficient variations in slopes or curvatures in the magnetic field to satisfy equation (17) and at the same time give reliable computational results.

Next, from equations (9) and (16c), we see that the best resolution is the product of σ and ΔT; that is, if we want to know the true magnetic susceptibility, we must know or assume the thickness of the dike, and vice versa. In fact, this is a well-known ambiguity in geophysics. For example, often we can only resolve the product of density and thickness in gravity problems, or resolve the product of conductivity and thickness in electromagnetic (EM) problems.

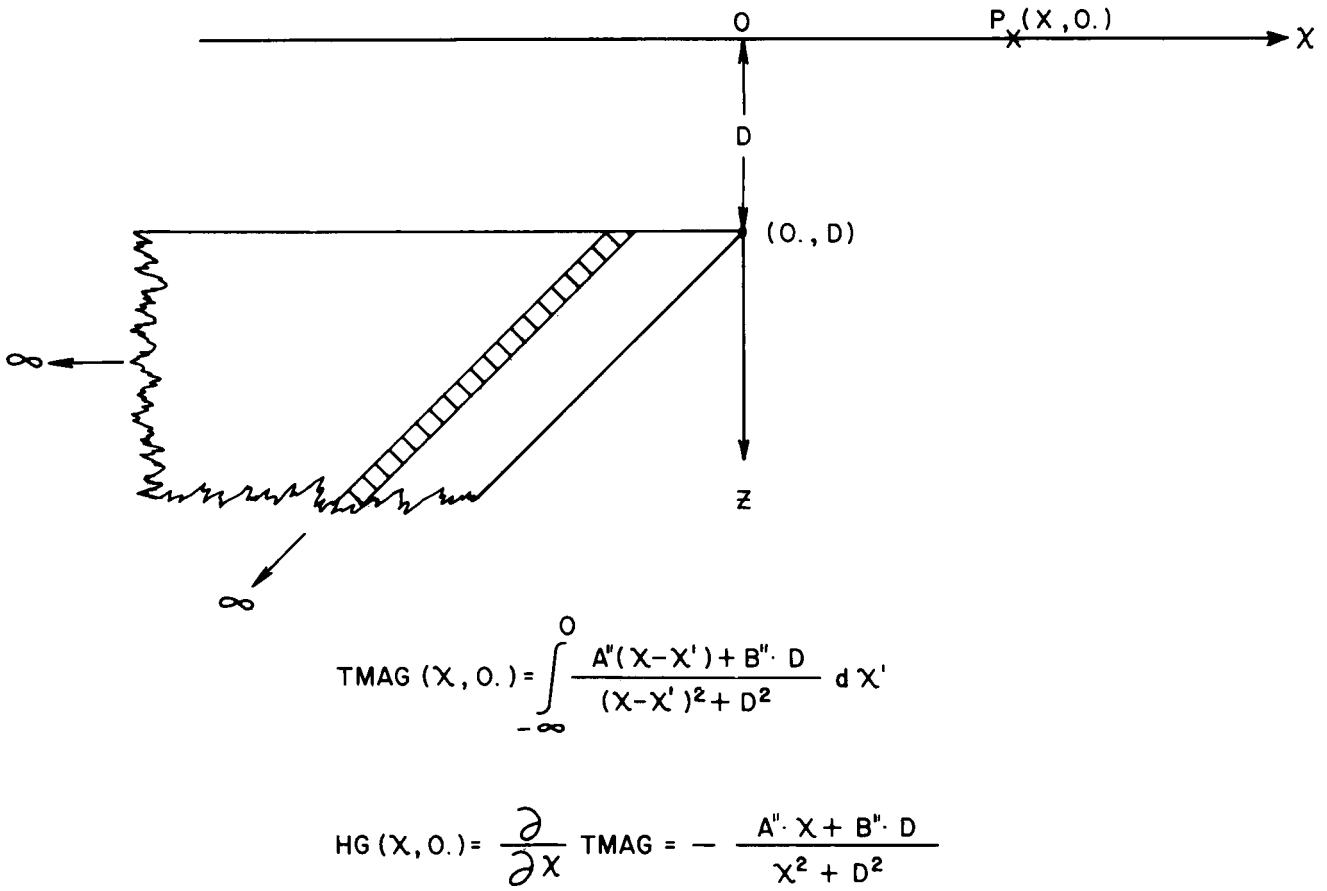

FIG. 2. Edge of a thick interface body showing dimensions and parameters. Extends to infinity in negative x direction.

Finally, as shown in Figure 1 and from equation (16d), the computed angle θ,

$$\theta = \tan^{-1}\left(\frac{J_x}{J_z}\right), \tag{18}$$

is in relation to the projection of the total field with apparent inclination I_a in the x-z plane. If we always choose the z-axis parallel to the body of the dike, and the x-axis perpendicular to it, then the dip angle computed from equation (16d) is generally valid for a dike dipping at any angle, so long as the dike is thin in comparison to its depth. The magnetization J_z which is parallel to the body of the dike but perpendicular to the top edge of the body is called the edge magnetization, whereas the magnetization J_x which is perpendicular to the body of the dike is called the cross magnetization by Werner.

Assume we have an appropriate Werner operator whose size is comparable to the size of an anomaly, and we sweep the operator across the anomaly. We will then obtain a group of continuous solutions when the operator straddles the anomaly. One might expect that the values of solutions would vary more or less depending upon the relative size and location of the operator with respect to the anomaly. In fact, the variations may be so large that we must discard some of the solutions. This is a very interesting and important statistical problem, and we discuss it in more detail later.

COMPUTED HORIZONTAL GRADIENT AND THE EDGE OF A THICK INTERFACE BODY

The validity of the Werner deconvolution technique is greatly expanded if we apply the Werner operator to the horizontal gradient of the total field as well as to the total field itself. In so doing, we are still looking at the same information but from a different point of view. The physical justification for this is quite simple yet very interesting.

The edge of a thick interface body can be considered to consist of a large number of parallel thin dikes. Hence, conceptually the magnetic anomaly caused by the edge involves an integration of the magnetic anomaly from a thin dike. If we take a differentiation in the form of a horizontal gradient, then the differentiation and the integration cancel. We end up with the same expression for the magnetic anomaly from a thin dike, except for a possible sign difference depending upon whether the edge is located at the left or right of the thick interface body. In other words, the horizontal gradient of the total field caused by the edge of a thick interface body is equivalent to the total field caused by a thin dike. This is a very useful concept when we apply the Werner operator

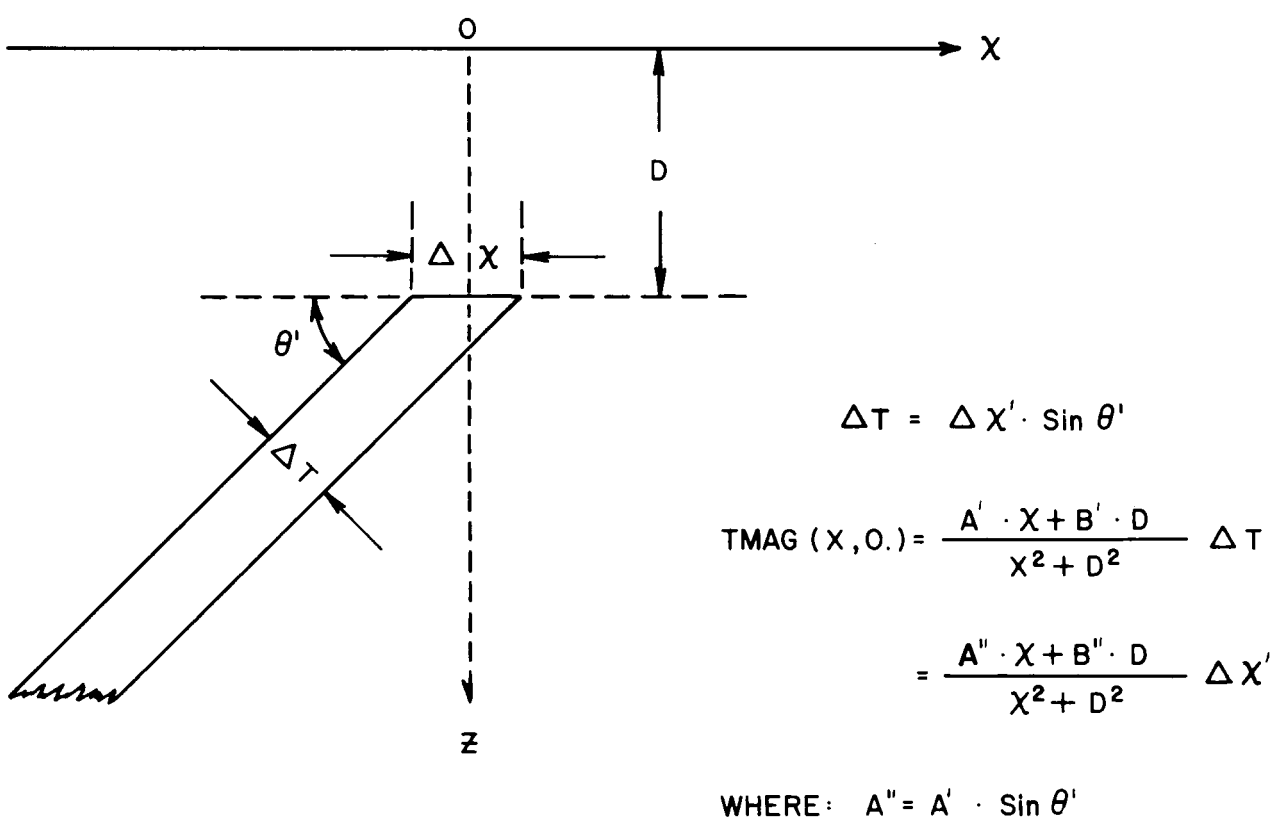

FIG. 3. Parameters of a 2-D inclined thin dike.

to the computed horizontal gradient of the total field for the purpose of resolving the edge of a thick interface body.

Let us consider the dipping edge of a thick interface body which extends to infinity both in the negative x-axis and the positive z-axis directions (Figure 2). For convenience, we let the top right-hand corner edge of the interface body be located at $(0, D)$. Now we can think of this thick interface body as being composed of an infinite number of infinitesimally thin dikes dipping parallel to the interface. In equations (7) and (8), let

$$A = A'\Delta T,$$
$$B = B'\Delta T,$$

and from Figure 3

$$\Delta T = \Delta x' \sin\theta',$$

or

$$A = A' \sin\theta' \Delta x' = A''\Delta x'$$
$$B = B' \sin\theta' \Delta x' = B''\Delta x'. \qquad (19)$$

From equations (10) and (19), the total magnetic anomaly caused by the edge of the interface is given by

$$\mathrm{TMAG}(x, 0) = \int_{-\infty}^{0} \frac{A''(x - x') + B''D}{(x - x')^2 + D^2}\, dx'.$$

It can be shown through coordinate transformation that the horizontal gradient of the total magnetic anomaly is given by

$$\frac{d}{dx}\mathrm{TMAG}(x, 0) = \frac{d}{dx}\int_{-\infty}^{0} \frac{A''(x - x') + B''D}{(x - x')^2 + D^2}\, dx'$$
$$= -\frac{A''x + B''D}{x^2 + D^2}. \qquad (20)$$

If the top corner edge of the interface is located at an arbitrary horizontal point $(x_0, 0)$, then

$$\frac{d}{dx}\mathrm{TMAG}(x, 0) = -\frac{A''(x - x_0) + B''D}{(x - x_0)^2 + D^2}. \qquad (21)$$

We can see that equations (20) and (21) are identical to equations (6) and (10) except for the sign difference. Thus, we can use the Werner horizontal-gradient solution to determine the depth, horizontal location, dip angle, and magnetic susceptibility of an interface, keeping in mind that the computed dip angle is in the opposite

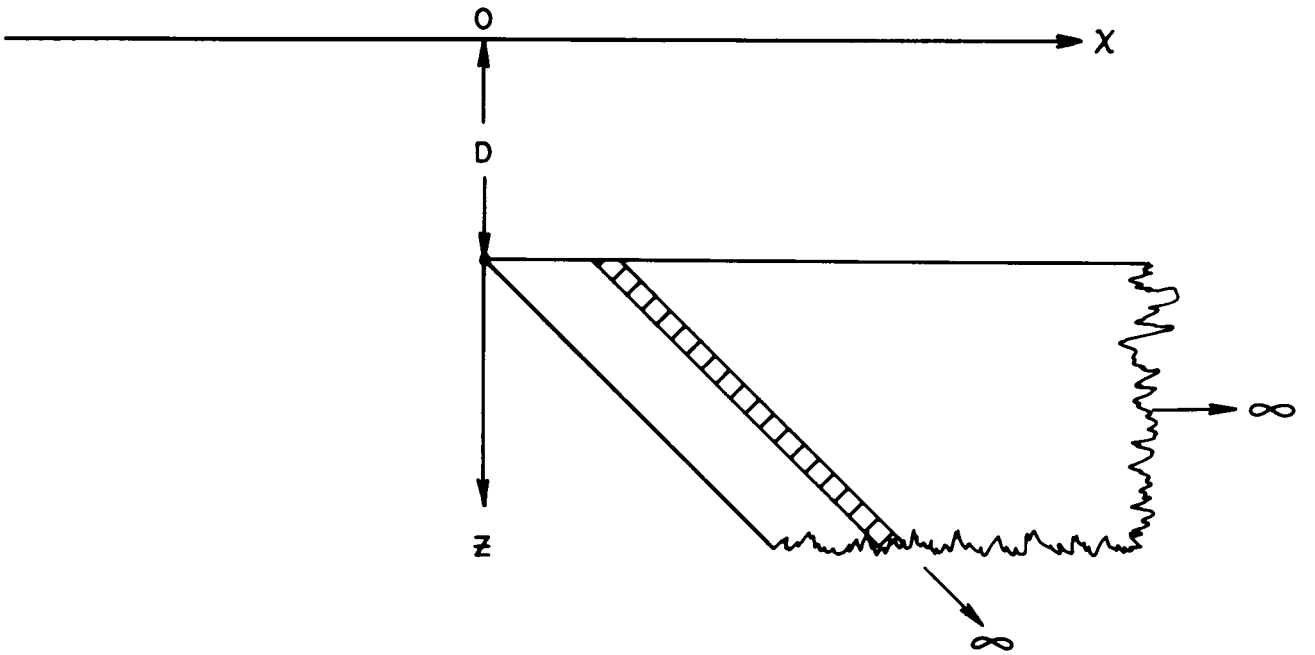

$$\text{TMAG}(X, 0.) = \int_0^{\infty} \frac{A''(X-X') + B'' \cdot D}{(X-X')^2 + D^2}\, dX'$$

$$\text{HG}(X, 0.) = \frac{\partial}{\partial X}\,\text{TMAG} = + \frac{A'' \cdot X + B'' \cdot D}{X^2 + D^2}$$

FIG. 4. Edge of a thick interface body showing dimensions and parameters. Extends to infinity in positive x direction.

direction from the true dip angle of the interface because of the negative sign in equations (20) and (21). It should also be pointed out that the computed magnetic susceptibility must be divided by sin θ' as seen from equations (9) and (19).

On the other hand, if the interface body extends to infinity in the positive x-axis direction as shown in Figure 4, then the horizontal gradient of the total field from the edge of such a body is given by

$$\frac{d}{dx}\,\text{TMAG}(x, 0) = \frac{A''(x - x_0) + B''D}{(x - x_0)^2 + D^2}, \qquad (22)$$

which is now identical to equation (10) including the sign. In this case, the dip angle computed from the horizontal gradient is the same as the true dip angle of the interface.

We have formally demonstrated that just as the Werner total-field solution is a good indicator of a thin-dike body, so is the Werner horizontal-gradient solution a good indicator of the edge of a thick interface body. Whereas the dip angle computed from the horizontal gradient can either be in the same or opposite direction to the true dip angle of the interface, the dip angle computed from the total field provides a clue in distinguishing between the two. Since the dip angle computed from the total field is 90 degrees ahead of (lead) that computed from the horizontal gradient, we can easily see from Figures 2 and 4 that the dip angle computed from the total field always points toward the interior of the interface body.

From Fourier transform theory, it can easily be shown that the computation of the horizontal gradient from the total field is simply a high-pass filtering operation with a multiplication factor of $i\omega$ in the frequency domain, where $i = \sqrt{-1}$ and ω is the angular frequency. This means that, in addition to the original total field spectrum being multiplied by the factor ω, there is also a 90-degree phase lag in the spectrum of the computed horizontal gradient with respect to the spectrum of the original total field. As a result, if we apply the Werner operator to the computed horizontal gradient, we expect that the Werner horizontal-gradient solution should be shallower in depth because of its higher frequency content, and it also should be perpendicular (90-degree phase lag) in dip angle to the Werner total-field solution.

To compute the horizontal gradient numerically from the recorded total field in digital form, the Lagrangian interpolation formula for seven points is used. Let TM1, TM2, . . . , TM7 be the values of total field at seven consecutive points x_1, x_2, . . . , x_7; then

$$\mathrm{TMAG}(x) = \frac{(x-x_2)(x-x_3)(x-x_4)\ldots,(x-x_7)}{(x_1-x_2)(x_1-x_3)(x_1-x_4)\ldots,(x_1-x_7)}\,\mathrm{TM1} + \frac{(x-x_1)(x-x_3)(x-x_4)\ldots,(x-x_7)}{(x_2-x_1)(x_2-x_3)(x_2-x_4)\ldots,(x_2-x_7)}\cdot \mathrm{TM2} + \ldots, + \frac{(x-x_1)(x-x_2)\ldots,(x-x_6)}{(x_7-x_1)(x_7-x_2)\ldots,(x_7-x_6)}\,\mathrm{TM7}.$$

To obtain the value of the horizontal gradient at $x = x_4$, for equal sample spacing $x = x_7 - x_6 = x_6 - x_5 = \cdots = x_2 - x_1 = 1.0$, we have

$$\frac{d}{dx}\mathrm{TMAG}(x_4) = \frac{(x_4-x_2)(x_4-x_3)\ldots(x_4-x_7)}{(x_1-x_2)(x_1-x_3)\ldots(x_1-x_7)}\,\mathrm{TM1} + \ldots, + \frac{(x_4-x_1)(x_4-x_2)\ldots(x_4-x_6)}{(x_7-x_1)(x_7-x_2)\ldots(x_7-x_6)}\,\mathrm{TM7}$$

$$= 0.0166667(\mathrm{TM7}-\mathrm{TM1}) - 0.15(\mathrm{TM6}-\mathrm{TM2}) + 0.75(\mathrm{TM5}-\mathrm{TM3}). \quad (23)$$

It should be noted that the above seven-point operator is antisymmetrical with respect to its center point at $x = x_4$, thus giving rise to a 90-degree phase shift in its operation, and also that the sum of the coefficients is zero because the multiplier $i\omega$ vanishes at $\omega = 0$ in the frequency domain.

INTERFERENCE, ITERATION, AND STATISTICAL DECISIONS

It should be apparent that the main feature of Werner deconvolution is its simplified thin-dike assumption which leads to the linearization of complex nonlinear magnetic problems. This linearity is retained even when we add interference terms in the form of a polynomial $C_0 + C_1x + C_2x^2$ to the total magnetic anomaly to take into consideration the main dipole field and regional

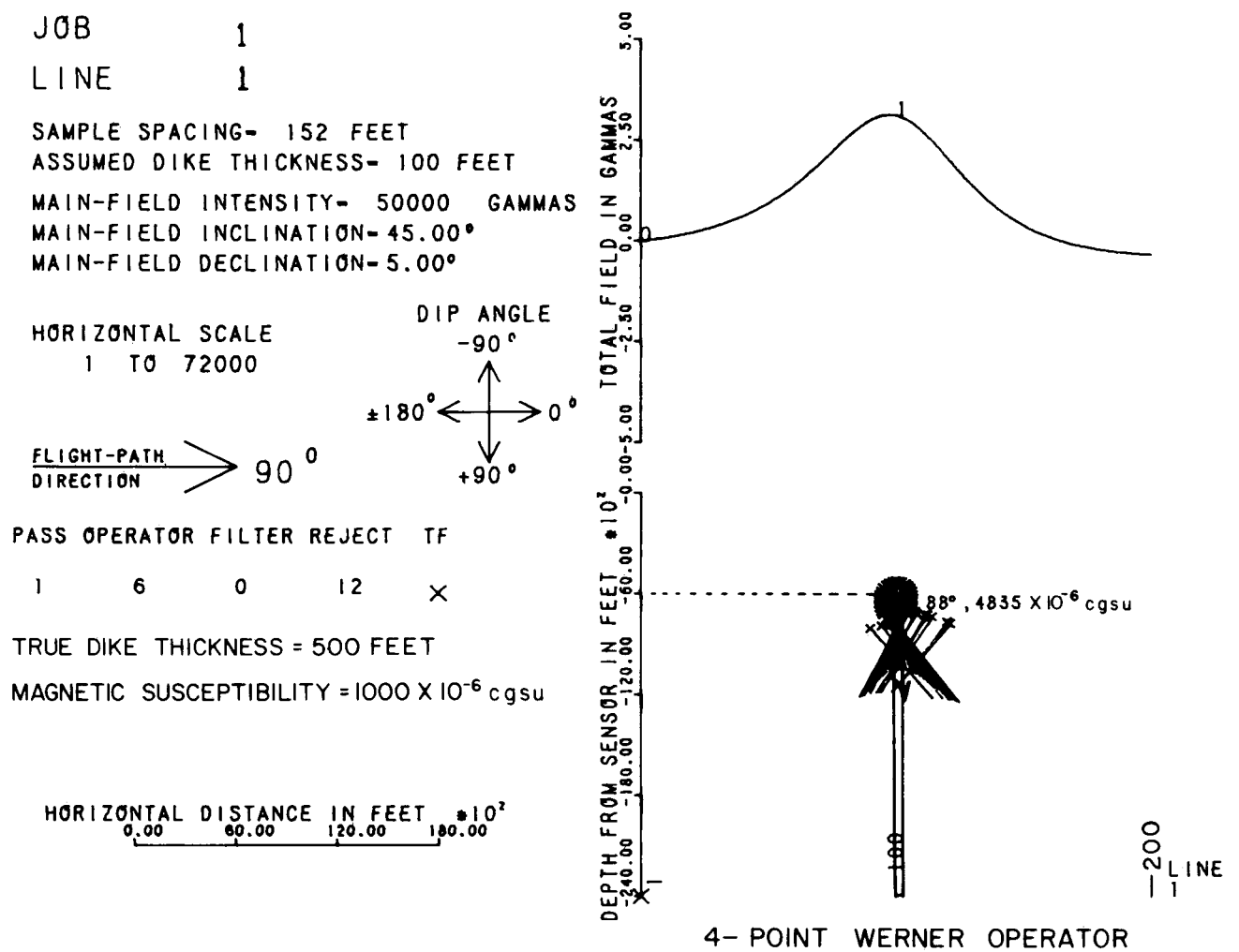

FIG. 5. Four-point Werner operator applied to magnetic anomaly caused by an ideal vertical thin dike.

gradient as follows:

$$\text{TMAG} = \frac{A(x - x_0) + BD}{(x - x_0)^2 + D^2} + C_0 + C_1 x + C_2 x^2. \quad (24)$$

Upon rearranging, we have:

$$a_0 + a_1 x + a_2 x^2 + a_3 x^3 + a_4 x^4 + b_0 \text{TMAG} + b_1 x\,\text{TMAG} = x^2 \text{TMAG} \quad (25)$$

where

$$\begin{aligned} a_0 &= -Ax_0 + BD + C_0 D^2 + x_0^2 C_0, \\ a_1 &= A - 2C_0 x_0 + C_1 D^2 + C_2 D^2, \\ a_2 &= C_0 - 2C_1 x_0 - C_2 x_0^2, \\ a_3 &= C_1 - 2x_0 C_2, \\ a_4 &= C_2, \\ b_0 &= -x_0^2 - D^2, \end{aligned}$$

and

$$b_1 = 2x_0. \quad (26)$$

Again we can see from equation (25) that we are still dealing with a linear problem but now with seven unknowns. Thus, if we know the value of TMAG at seven appropriate points, we should be able to obtain the values of these seven unknowns simply by solving seven simultaneous linear equations. In terms of these unknowns, we have

$$\begin{aligned} x_0 &= 0.5\, b_1, \\ D &= \sqrt{-b_0 - x_0^2}, \\ C_2 &= a_4, \\ C_1 &= a_3 + 2x_0 C_2, \\ C_0 &= a_2 + 2C_1 x_0 + C_2 x_0^2, \\ A &= a_1 + 2C_0 x_0 - C_1 D^2 - C_2 D^2, \end{aligned}$$

and

$$B = \frac{1}{D}[a_0 + Ax_0 - C_0 D^2 - C_0 x_0^2]. \quad (27)$$

It should be emphasized here that to compute the magnetizations

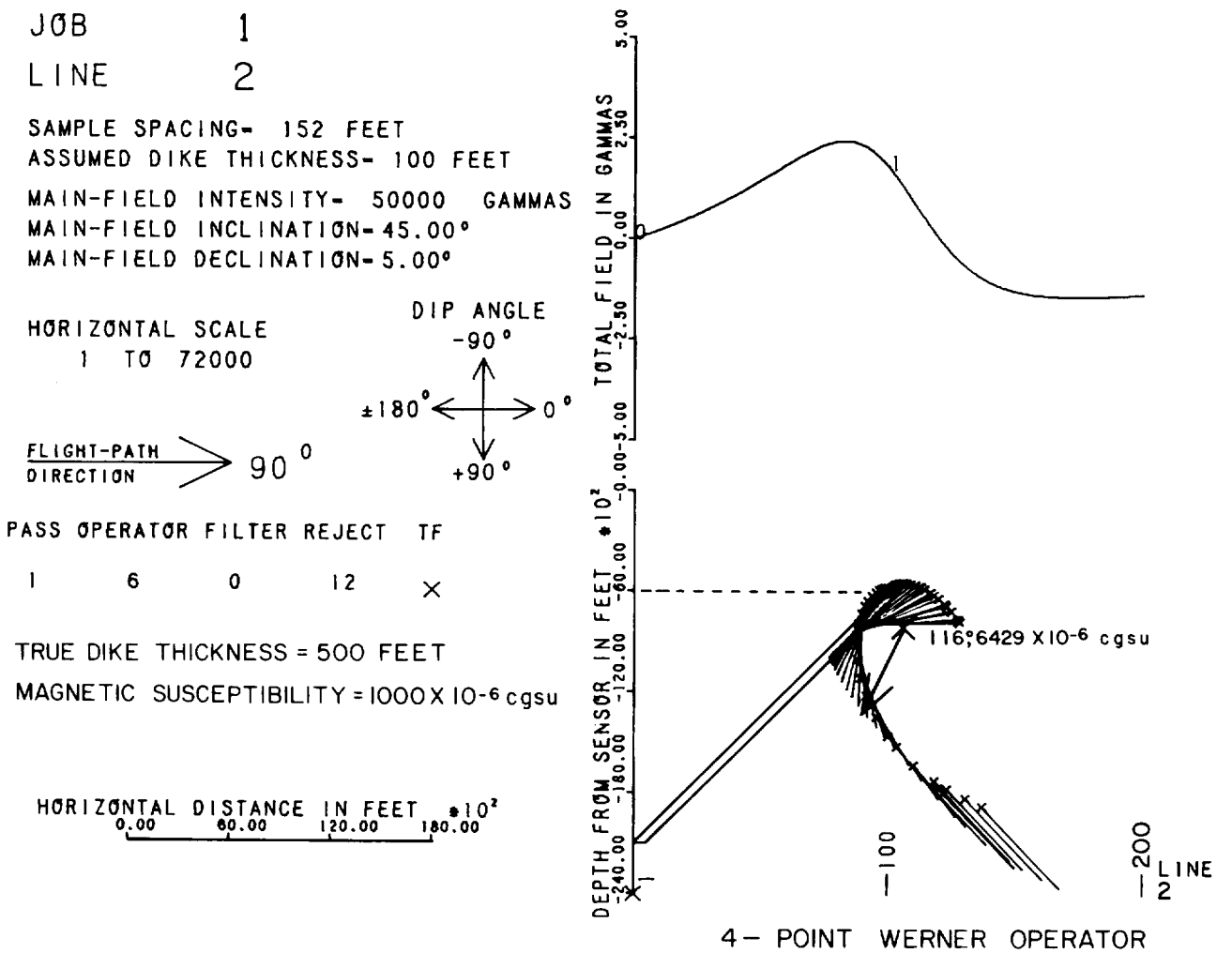

FIG. 6. Four-point Werner operator applied to magnetic anomaly caused by an ideal inclined thin dike.

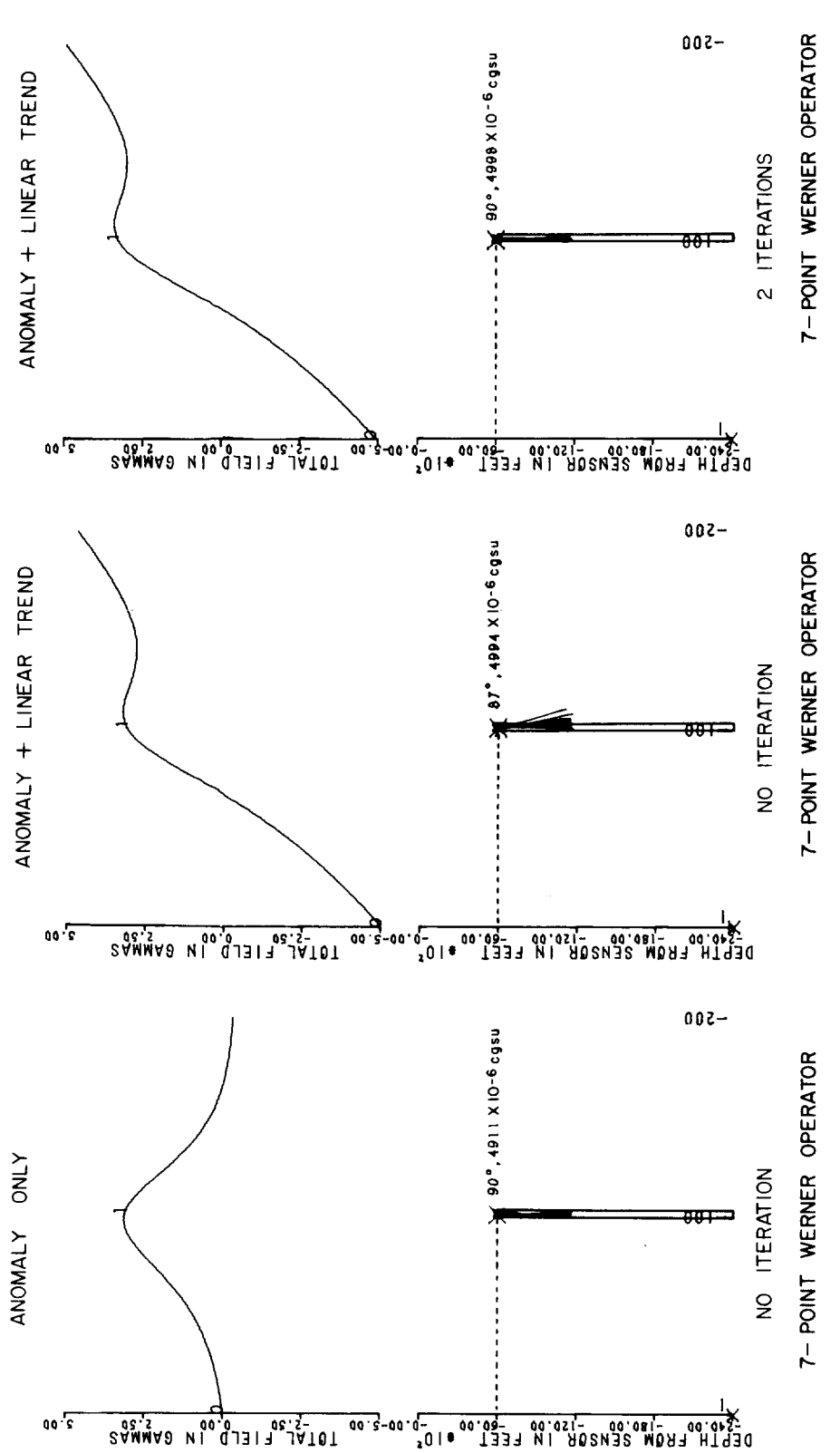

FIG. 7. (a) Seven-point Werner operator applied to magnetic anomaly caused by an ideal vertical thin dike. (b) Seven-point Werner operator applied to the same magnetic anomaly superimposed on a linear trend. No numerical iteration. (c) Seven-point Werner operator and 2 numerical iterations applied to the magnctic anomaly superimposed on a linear trend.

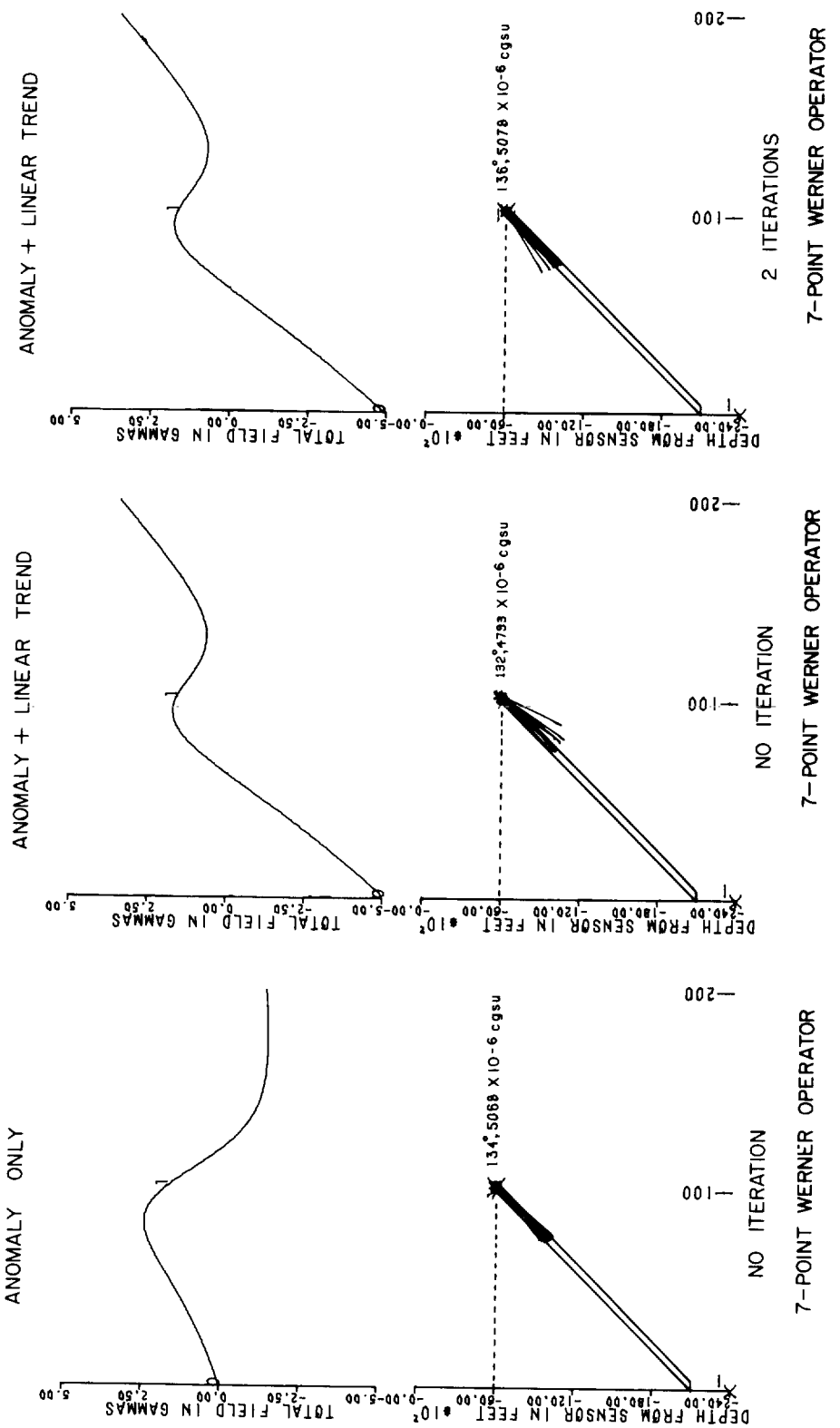

FIG. 8. (a) Seven-point Werner operator applied to magnetic anomaly caused by an inclined thin dike. (b) Seven-point Werner operator applied to the same magnetic anomaly superimposed on a linear trend. (c) Seven-point Werner operator and 2 numerical iterations applied to the magnetic anomaly superimposed on a linear trend.

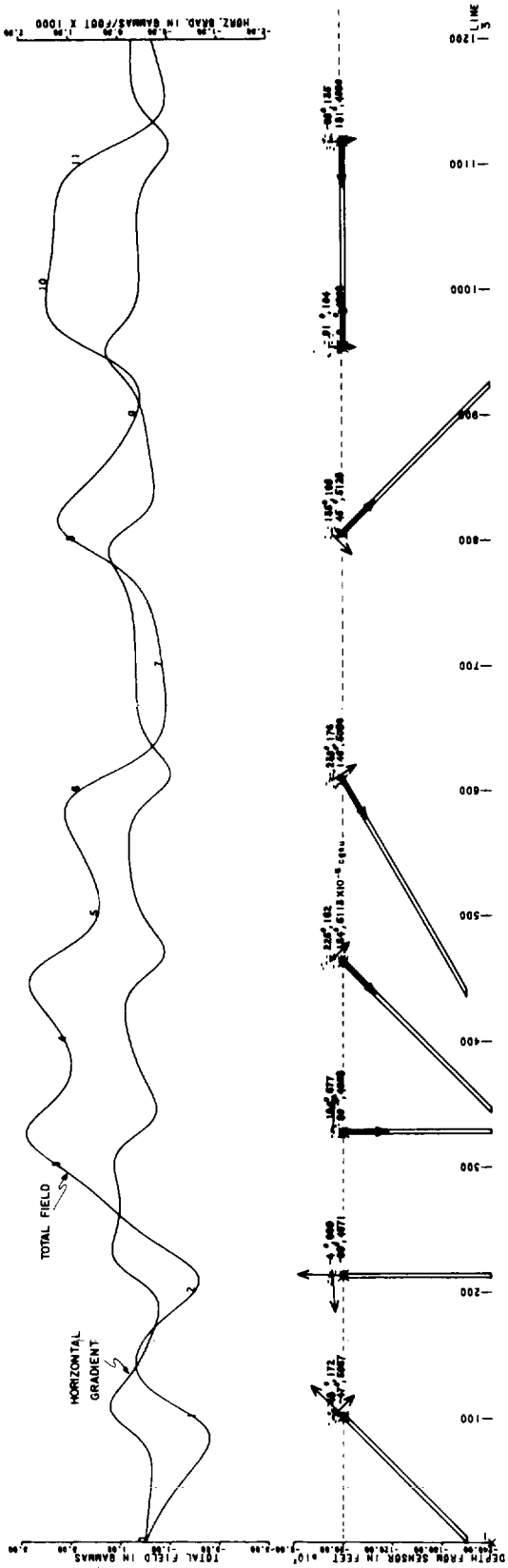

FIG. 9. Seven thin dikes inclined at various angles with respect to a horizontal ground surface, 500 ft thick, susceptibility contrast 1000×10^{-6} cgsu, buried 6000 ft below the sensor. Solutions computed using a seven-point Werner operator, numerical iterations, and statistical decision.

J_x and J_z we must use equation (9) and the values of A and B in equation (27), not equation (15). Equation (15) only applies to the four-point Werner operator. Later in this section we demonstrate that the four-point operator does not work as well as the seven-point operator.

We made a minor improvement in dealing with equation (24) using a simple numerical iteration as follows. In general, we are not interested in the interference coefficients C_0, C_1, and C_2 which represent the main dipole field, and first- and second-order terms superimposing on the magnetic anomaly of interest. After first computing the values of C_0, C_1, and C_2, we subtract these values from the total field TMAG in equation (24) to reduce and possibly to eliminate the effects of interferences, and obtain a set of new TMAG values which are more representative of the magnetic anomaly itself. New values of C_0, C_1, and C_2 are again computed from the new TMAG values, and they are once again removed from the new TMAG values. By repeating the process, we end up with very small or nearly zero values of C_0, C_1, and C_2, indicating that we have reduced the interferences and isolated the magnetic anomaly we want to analyze. The magnetic parameters computed from the iterated TMAG values generally yield much more accurate results than those from the original TMAG values.

In the following, we show the differences between the four-point Werner operator and the seven-point Werner operator, and we also show the improvements made from using iterations and some simple statistical decisions.

Let us see what would happen if we applied a four-point Werner operator to an ideal vertical thin dike as shown in Figure 5. The dike is 6000 ft deep, 500 ft wide, and the sample spacing is 152 ft between observation points (fiducials). The total magnetic anomaly caused by the dike is about 120 fiducials wide, although we show a profile of 200 fiducials total. The Werner decimation operator size is 6 fiducials wide, thus giving rise to Werner total-span operator size of $(4 - 1) \times 6 = 18$ fiducials, which is only 0.15 the magnetic anomaly size. As we sweep the four-point Werner operator from left to right as in Figure 5, we see a series of solutions whose depths are indicated by cross symbols, dip angles by straight-line segments, and magnetic susceptibility by the length of the line segments. Since the formula we use for Werner deconvolution is for a vertical dike, the Werner total-field solutions yield dip angles which are more or less perpendicular to the part of the total field curve straddled by the Werner operator. Thus the dip angles rotate clockwise from dipping to the right to dipping to the left in accordance with the normal direction of the total field curve.

If we apply the four-point Werner operator to the total field from an inclined thin dike as shown in Figure 6, we can see that the dip angles still rotate clockwise in the same sense as those for the vertical dike in Figure 5. However, the left part of the total field curve, being flatter because of the negative skewness to the left, yields much deeper solutions than the true depth of the dike.

Now apply a seven-point Werner operator to the same vertical and inclined dikes shown previously. We use the same Werner decimation operator size of 6 fiducials, which gives rise to a total-span operator size of $(7 - 1) \times 6 = 36$ fiducials, which is about 0.3 the magnetic anomaly size. When we apply the seven-point operator to the total field (anomaly only) caused by the vertical dike as shown in Figure 7a, we can see that the Werner solution yields very accurate computations with respect to depth, horizontal position, dip angle, and susceptibility of the dike, indicating that the seven-point operator is needed even when the magnetic anomaly is present by itself. On the other hand, when the magnetic anomaly is sitting on a linear trend as in Figure 7b, we see that the dip angle based on the Werner solution is tilted to the right, much the same way the magnetic anomaly is tilted to the right. However, if we apply iterations in our Werner deconvolution as shown in Figure 7c, we can see that the Werner solution now yields much more accurate computations.

Similar results are obtained when we apply the seven-point operator to the inclined dike as shown in Figures 8a, 8b, and 8c. However, we can see from Figure 8c that there are still two separate solutions which are slightly off from the true dip of the inclined dike. We intentionally show Figure 8c to demonstrate that although iterations will generally lead to tighter grouping, we also need a simple statisical decision to improve our computation. We use two standard deviations from the mean values of depth, horizontal position, susceptibility, and dip angle as rejection criteria in computing Figure 8c, and the two off-solutions could be removed simply by using a cut-off of one standard deviation instead.

In short, the higher order terms in the form of a seven-point operator, or at least a six-point operator, are needed in order to see a magnetic anomaly accurately as well as to reduce interferences from the main dipole field and regional trends which are generally not of exploration interest. These higher order terms also provide compensation when the thin dike is not vertical, thus intersecting with the line of observation at an angle other than 90 degrees. Although we used an operator that is slightly too small in the previous examples, the desirable operator size should actually be from one-half to full size of the magnetic anomaly under deconvolution. Since the Werner operator is able to see double peaks or double troughs, one should be careful not to use too big an operator in order to avoid erroneous calculations. In general, two iterations are sufficient to reduce the interferences, and a cut-off of one standard deviation should be enough to improve computational results.

MODELS

As indicated above, the Werner total-field solution provides a very close approximation when the geologic body is an infinitely long thin dike, whereas the Werner horizontal-gradient solution provides a very close approximation when the body is the edge of a thick interface. Hence it is only natural for us to consider thin dikes and the edges of thick interfaces as our first models to test the validity of the Werner deconvolution technique. We then investigate the behavior of Werner deconvolution on geologic bodies which vary transitionally from a thin dike to the edge of a thick interface. Finally, we consider geologic bodies which are neither thin dikes nor the edges of thick interfaces, but simply high- and low-basement topographic relief.

Thin dikes

In Figure 9 we consider seven thin dikes each dipping at a different angle with respect to a horizontal ground surface. Each dike is 500 ft thick with a susceptibility contrast of 1000×10^{-6} cgsu buried at a depth of 6000 ft below the sensor. For ease of discussion we numbered the dikes 1 through 7 from left to right. Dikes 1 and 2 represent reverse polarized bodies (negative susceptibility contrast) dipping at 45 and 90 degrees, respectively. The other dikes shown on the line possess positive susceptibility contrasts but dip at different angles. Dikes 3 through 7 dip at 90, 135, 150, 45, and 180 degrees, respectively. Note that dike number 7, which dips horizontally, represents a horizontal thin sheet.

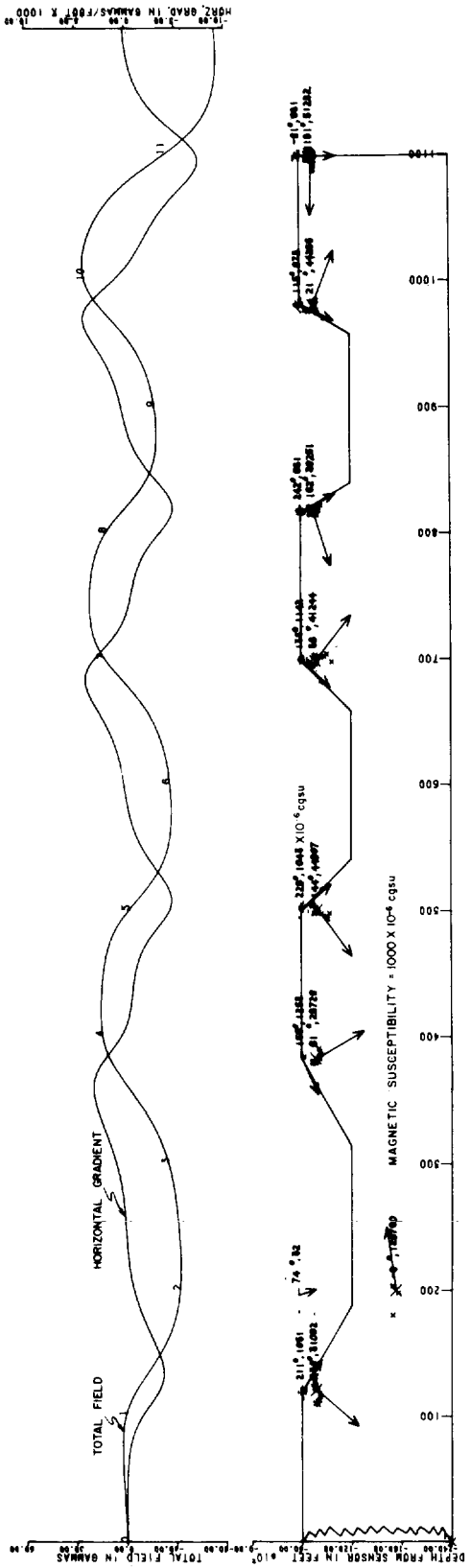

FIG. 10. Seven interfaces representing normal faults inclined at various angles with respect to a horizontal ground surface, susceptibility contrast 1000×10^{-6} cgsu, buried 6000 ft below the sensor. Solutions computed using a seven-point Werner operator, numerical iteration, and statistical decision.

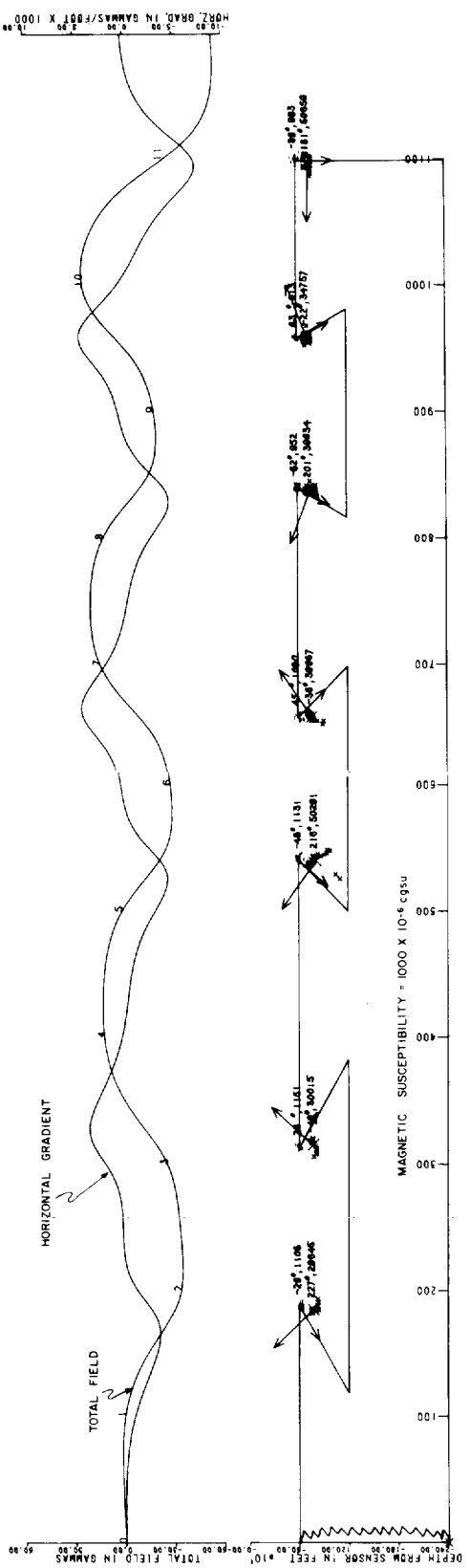

FIG. 11. Seven interfaces representing reverse faults inclined at various angles with respect to a horizontal ground surface, susceptibility contrast 1000×10^{-6} cgsu, buried 6000 ft below the sensor.

All seven of the above dikes represent commonly occurring geologic bodies of exploration interest.

The total field profile was computed using Talwani and Heirtzler's (1964) method, and the horizontal gradient was computed using the seven-point formula given in equation (23). The line is a total of 1200 fiducials long, with the sample spacing between consecutive fiducials equal to 152 ft. From visual inspection of the shape of the total field and the horizontal gradient, the main magnetic anomaly caused by each dike spans about 50 fiducials. Since the seven-point Werner operator is used, the desired Werner decimation operator size is $50/(7 - 1) = 8$ fiducials (operator applied to every eighth fiducial). To avoid interference from adjacent dikes, we slightly reduce the Werner decimation operator size to 6 fiducials. Thus, the Werner total-span operator size is $(7 - 1) \times 6 = 36$ fiducials, which is approximately two-thirds the size of the magnetic anomalies from each thin dike.

The total-field solution is represented by a group of crosses, whereas the horizontal-gradient solution is represented by a group of horizontal bars. Their mean values are indicated by the large crosses and bars associated with two numbers and an arrow: the first number gives the computed dip angle, and the second number computed magnetic susceptibility in $\times 10^{-6}$ cgsu; the origin of the arrow indicates the computed mean horizontal location and depth of the dikes. In general, when the Werner operator straddles a magnetic anomaly, we should obtain a group of solutions as wide as the anomaly size. To be conservative, we use 12 consecutive solutions as our rejection criterion, that is, when the number of solutions is less than 12, that particular group of solutions is discarded.

Since our models are all thin dikes, we concentrate on the total-field solutions which quite accurately represent the dikes in terms of depth, horizontal location, dip angle, and magnetic susceptibility. Note that we assume the thickness of the dikes is 100 ft instead of the true thickness of 500 ft; thus the computed susceptibility, being about 5000×10^{-6} cgsu, is roughly 5 times larger than the true susceptibility of 1000×10^{-6} cgsu. We also note that since dikes 1 and 2 have negative susceptibility, the computed dip angles are in the opposite direction to the dip angle of the other dikes.

It is interesting to note that the computed dip angles and susceptibility contrasts shown for dikes 1 through 7 closely match the actual values used in generating the total field profile. In fact, the dip angles are within 3 degrees of the true value, and the susceptibility contrast is within 5 percent once we take into account a dike thickness of 500 ft. The set of dike models presented in this section demonstrates quite clearly that the computed depths, dips, susceptibility contrasts, and horizontal locations are all within 5 percent or better of the actual values.

Edges of thick interfaces

In Figures 10 and 11 we model seven interfaces dipping at increasingly steeper angles toward the right in order to simulate normal and reverse faults. The sources are buried at a depth of 6000 ft below the sensor with susceptibility contrasts of 1000×10^{-6} cgsu. Notice from both figures that for the interfaces the horizontal-gradient solutions are tightly grouped, as compared with the total-field solutions which give tight groupings for the dike sources. In addition, the depths estimated from the total field are consistently deeper than the horizontal gradient solutions. In fact, they are generally about 20 percent deeper. Since we are dealing with interfaces, the depths associated with the horizontal gradients are the correct choice. Besides being a good approximation in depth and horizontal location, we can also see that the computed dip angles are consistently within 4 degrees of the true dip angles, and the computed susceptibility contrast within 5 percent of the true value.

It should be pointed out that the Werner operator detects only the top edge of the interfaces because their dip angles are mostly greater than 30 degrees such that the horizontal separation between the top edge and the bottom edge of a given interface is not large enough to be seen as two separate magnetic anomalies. One exception to this is the first interface of Figure 10 in which the normal fault face dips at an angle of 30 degrees. In this case the horizontal separation between the bottom and top edge of the interface is large enough so that the Werner operator can partially recognize the effect of the bottom edge. From the figure we can see that the Werner solutions symmetrically bracket the actual bottom interface edge. Although the bottom interface is not well defined, it still serves to illustrate that the Werner method has the capability to resolve depth to bottom in certain situations.

Transition from a thin dike to the edge of a thick interface

It is interesting to examine the behavior of the Werner total-field operator and the horizontal-gradient operator on geologic bodies which vary transitionally from a thin dike to the edge of a thick interface as shown in Figure 12. We have numbered the bodies from 1 to 6 from left to right. Since the width of the bodies varies, we use three different Werner operator sizes of 5, 8, and 12 fiducials to cover similar variations of the anomaly size.

Compared with its depth, body 1 is a typical vertical thin dike which is well defined by the total field solutions with a very tight grouping. As the width of the geologic bodies increases from body 2 to body 4, we observe an increase in the spread of the total-field solutions and also a shift of the true depth from the total-field solution depth to the horizontal-gradient solution depth. Note that the width of body 4 is the same as its depth. Thus the thin dike assumption is no longer valid; yet it is interesting to see that the spread in its total-field solutions is roughly the same as the width of the body. For body 5, when the width is about 1.5 times its depth, we obtain 2 groups of solutions, indicating that the anomaly is just wide enough to be resolved into two separate parts for the edges, but still too narrow to yield good horizontal-gradient solutions for the edge of an interface. Finally, for body 6 we see that the edges are well indicated by the rather tightly grouped horizontal-gradient solutions.

Simple high- and low-basement topographic relief

Finally, let us see what the Werner operator will do when the geologic bodies are neither thin dikes nor the edges of thick interfaces, but simply high- and low-basement topographic relief with depth increasing from 6000 ft at the left to 12,000 ft at the right. In Figure 13 we use four Werner decimation operator sizes of 5, 8, 12, and 25 fiducials to cover different anomaly sizes corresponding to different depths of the geologic bodies.

It appears that the simple high and low topographic relief can still be considered as the edge of an interface at very low angles (less than 20 degrees), so that the horizontal-gradient solution is more indicative of the true depth of the bodies. The dip direction of the total-field solution is indicative of whether a body is a "hill" if it dips downward or a "valley" if it dips upward. As expected, the deeper the bodies, the larger the Werner operator size should be in order to see the bodies.

In this section, we use several different models to demonstrate the validity of the Werner deconvolution. We note that the true

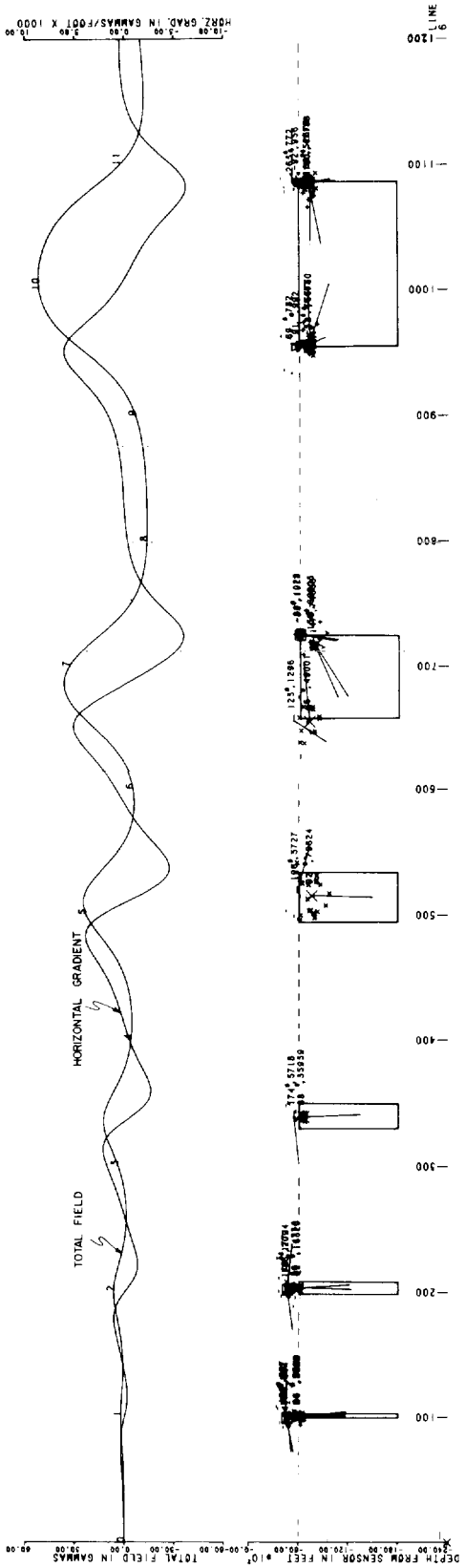

FIG. 12. Werner deconvolution applied to geologic bodies which vary transitionally from thin dikes to edges of interfaces.

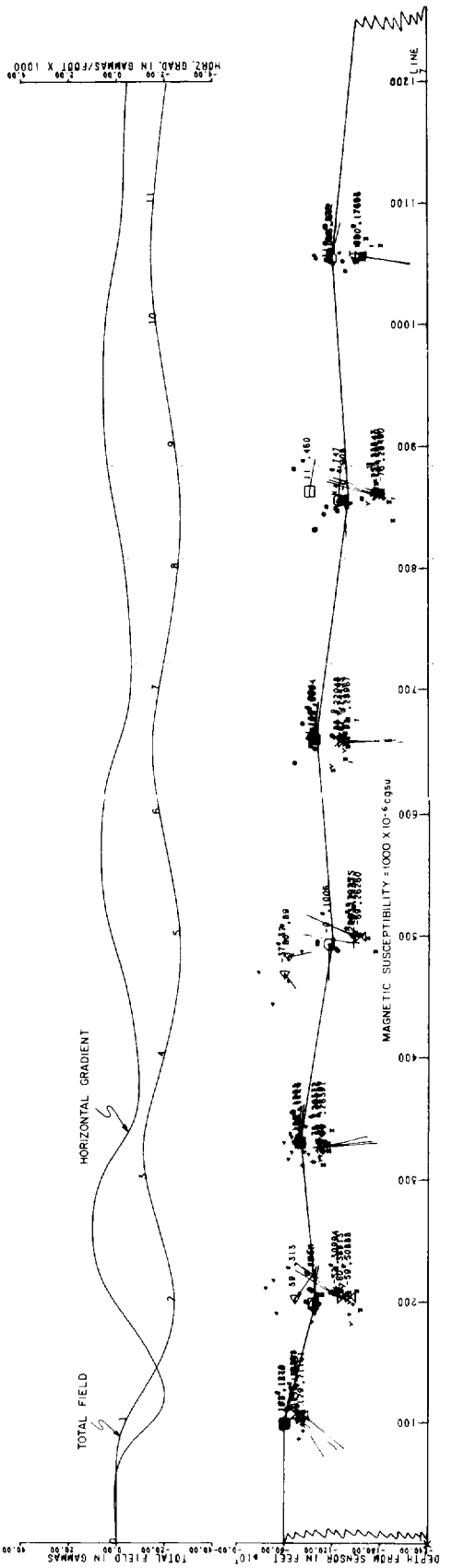

FIG. 13. Werner deconvolution of high- and low-basement topographic relief varying in depth from 6000 ft on the left to 12,000 ft on the right.

depth in most cases lies somewhere between the limits of the total-field depth solution and the horizontal-gradient depth solution. We also observe that the spatial spread in grouping is a good indicator as to the type of geologic body we might be dealing with. As a general rule, by looking at the magnetic anomaly width and using geophysical common sense, a tight grouping in total-field solutions with a narrow magnetic anomaly width suggests that the geologic body is a thin dike, whereas a tight grouping in horizontal-gradient solutions on the edge of a wide magnetic anomaly suggests that the geologic body is the edge of an interface. A wide spread in grouping both in total-field and horizontal-gradient solutions over an entire magnetic anomaly width might indicate that the geologic body is something in between the above two extreme types of bodies. It should be emphasized, however, that the wide spread in the grouping should not necessarily be considered bad since our thin-dike assumption is certainly an oversimplification; in fact, it is a blessing in the sense that the spread itself usually depicts the outline of the body. On the other hand, using linear filtering might lead to a tighter grouping as a result of smoothing of the magnetic anomaly, but this smoothing is certainly undesirable because it yields deeper depth solutions as well as erroneous dip and susceptibility computations.

MARQUARDT'S NONLINEAR LEAST-SQUARES BEST FIT APPROACH

The inverse problem is common in many geophysical applications (Wu, 1968; Johnson, 1969; McGrath and Hood, 1973; Ku, 1976). Basically, there are two methods that can be used for this purpose. Suppose we have m sets of observed values G_i, which can also be approximately fitted by m sets of theoretical values F_i. In the Gauss method (or Taylor series method), the function F_i is expanded into a truncated Taylor series with respect to n number of unknown parameters b_j by discarding higher order terms including the second derivatives:

$$F_i = f_i + \sum_{j=1}^{n} \Delta b_j \frac{\partial f_i}{\partial b_j}, \quad i = 1, \ldots, m. \tag{28}$$

Taking the sum of the squares of the differences between the theoretical values F_i and the observed values G_i, we obtain the variance

$$\Phi = \sum_{i=1}^{m} (F_i - G_i)^2 = \sum_{i=1}^{m} \left(f_i + \sum_{j=1}^{n} \Delta b_j \frac{\partial f_i}{\partial b_j} - G_i \right)^2. \tag{29}$$

Our goal is to minimize Φ in equation (29) by setting

$$\frac{\partial \Phi}{\partial \Delta b_k} = 0, \quad k = 1, \ldots, n. \tag{30}$$

In general, the m number of observations is larger than the n number of unknown parameters; thus equation (30) is solved in the least-squares sense.

For simplicity, let us consider the first unknown parameter b_1, upon substituting equation (29) into equation (30),

$$\frac{\partial \Phi}{\partial \Delta b_1} = 0 = \frac{\partial}{\partial \Delta b_1} \sum_{i=1}^{m} \left(f_1 + \sum_{j=1}^{n} \Delta b_j \frac{\partial f_i}{\partial b_j} - G_i \right)^2,$$

and

$$\sum_{i=1}^{m} \frac{\partial f_i}{\partial b_1} \sum_{j=1}^{n} \Delta b_j \frac{\partial f_i}{\partial b_j} = - \sum_{i=1}^{m} \frac{\partial f_i}{\partial b_1} (f_i - G_i). \tag{31}$$

Since we have n unknown parameters, we have n sets of equations in the form of equation (31) which can be simplified into matrix notation as follows:

$$[\mathbf{A}][\Delta \mathbf{b}] = [\mathbf{G}]. \tag{32}$$

From equation (31), we can easily see that the matrix $[\mathbf{A}]$ in equation (32) involves only multiplication of the partial derivatives $\partial f_i/\partial b_j$, whereas the matrix $[\mathbf{G}]$ involves multiplication of the partial derivatives $\partial f_i/\partial b_j$ and the differences $(f_i - G_i)$. In this paper, the values of the partial derivatives $\partial f_i/\partial b_j$ are numerically computed by increasing the current values of the unknown parameters b_j by 1 percent. In as much as the unknown parameters are often in different dimensions or units, the values of the partial derivatives $\partial f_i/\partial b_j$ range widely and are incompatible. Thus the matrix $[\mathbf{A}]$ in equation (32) must be normalized by setting its diagonal elements equal to unity. Furthermore, the original values of the diagonal elements are generally a maximum because they consist only of squared terms (all positive)

$$\sum_{i=1}^{m} (\partial f_i/\partial b_k)^2, \quad k = 1, \ldots, n,$$

whereas the other nondiagonal elements tend to be smaller because they consist of cross terms (positive and negative cancel each other)

$$\sum_{i=1}^{m} (\partial f_i/\partial b_k)(\partial f_i/\partial b_1), \; k \neq h, \; k \text{ and } h = 1, \ldots, n.$$

After normalization of the diagonal elements into unity, the nondiagonal elements would be smaller than unity, making $[\mathbf{A}]$ in equation (32) a well-behaved matrix. Now by a simple matrix inversion, the correction vector $[\mathbf{b}]$ in equation (32) can readily be obtained and added to the current values of unknown parameters to form a new set of unknown parameters in a vector form

$$[\mathbf{b}] = [\mathbf{b}] + [\Delta \mathbf{b}].$$

The process is repeated until the theoretical values f_i are close to the observed values G_i within a prescribed limit or after a certain number of iterations, whichever comes first.

In the steepest descent method, we simply step off from the current trial values of unknown parameters b_j in the direction of negative gradient of Φ_0.

$$[\Delta b_0] = - \left[\frac{\partial \Phi_0}{\partial b_1}, \frac{\partial \Phi_0}{\partial b_2}, \ldots, \frac{\partial \Phi_0}{\partial b_n} \right], \tag{33}$$

where

$$\Phi_0 = \sum_{i=1}^{m} (f_i - G_i)^2. \tag{34}$$

Again for simplicity, let us consider the first unknown parameter b_1, and upon taking the derivative of Φ_0 in equation (34) with respect to b_1, we have

$$- \frac{\partial \Phi_0}{\partial b_1} = \frac{-\partial}{\partial b_1} \sum_{i=1}^{m} (f_i - G)^2 = -2 \sum_{i=1}^{m} \frac{\partial f_i}{\partial b_1} (f_i - G_i). \tag{35}$$

Equation (35) is equal to the right-hand side of equation (31)

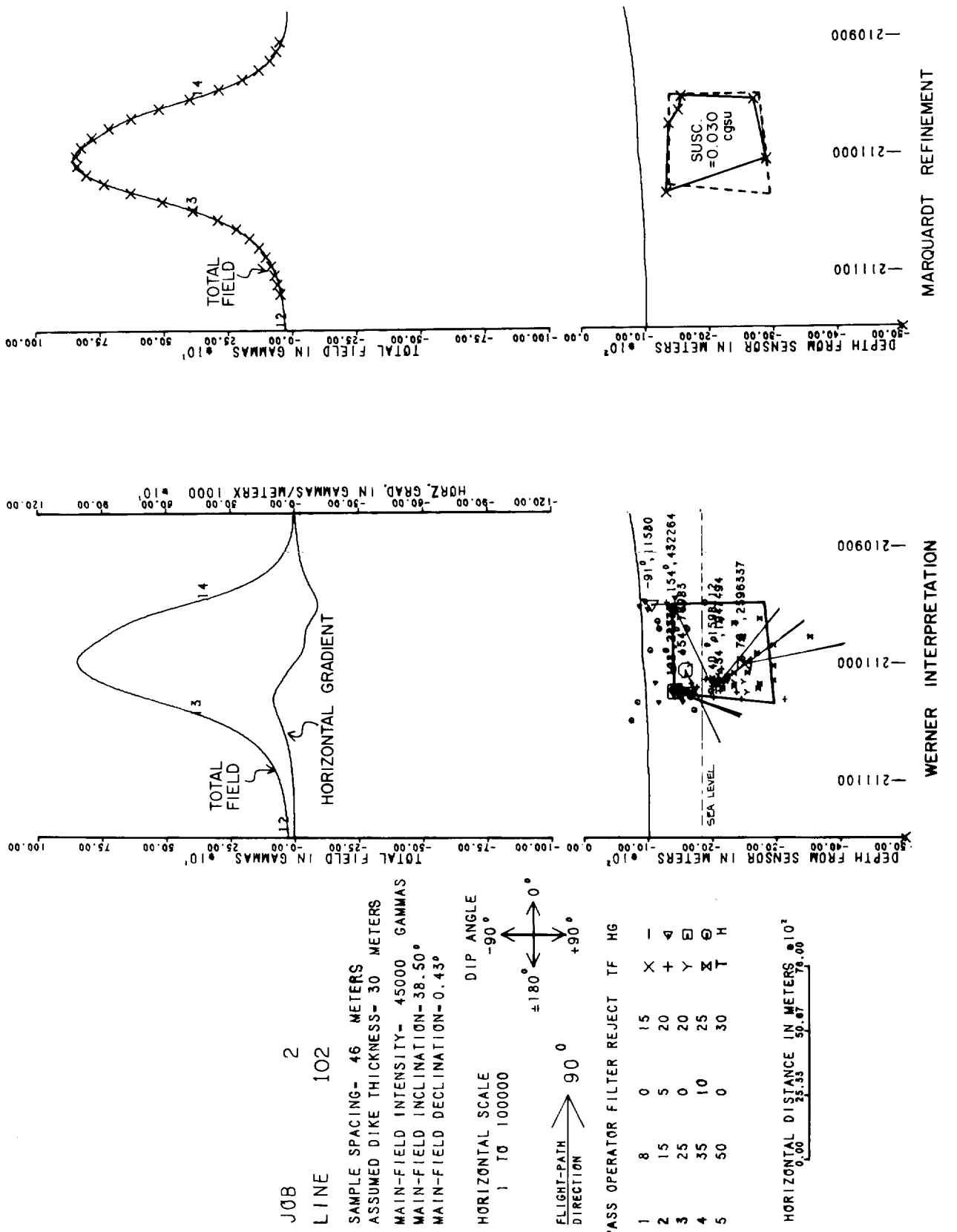

FIG. 14. Werner deconvolution and Marquardt refinement of a basement anomaly.

except for the factor of 2. This important relation constitutes the basis of the Marquardt method (1963) which combines both advantages from the Gauss method and the steepest descent method. The steepest descent method guarantees the convergence of the solution if the initial guess for the unknown parameters is within reasonable range of the true values. Its main disadvantage is that the rate of convergence becomes very slow after the first few iterations. The Gauss method, on the other hand, may yield a rapid rate of convergence, but it often suffers from a failure to converge.

Marquardt ingeniously took advantage of the above two basic methods by adding another term in equation (32)

$$([\mathbf{A}] + \lambda[\mathbf{I}])[\Delta\mathbf{b}] = [\mathbf{G}], \tag{36}$$

where $[\mathbf{I}]$ is an identity matrix. It is obvious that when $\lambda = 0$, the Marquardt method reduces to the Gauss method, whereas when λ is larger than unity, say $\lambda \geq 10$, then equation (36) becomes

$$[\Delta\mathbf{b}] \cong \frac{2}{\lambda}[\mathbf{G}], \tag{37}$$

which is equal to the steepest descent method of equation (33) except for the factor of $2/\lambda$. In other words, Marquardt's method approaches the steepest descent method so far as the directions of their correction vectors are concerned, but the magnitude of the correction from the Marquardt method is smaller than that from the steepest descent method by the factor of $2/\lambda$, where $\lambda \geq 10$.

Thus in the Marquardt method, we initially set λ larger than unity, taking advantage of the steepest descent method that will assure the convergence. At the end of each iteration, λ is reduced to some reasonable number (say by a factor of 10), hence moving toward the Gauss method so as to increase the rate of convergence. In the process, especially after a few iterations and when the value of λ is much smaller than unity (say $\lambda = 0.0001$), we might find that the iteration is diverging instead of converging. In that case, we reset the value of λ larger than unity, and restart our iteration. Indeed, we can even cut down the number of iterations by setting the starting or resetting value of λ less than unity (for example, $\lambda = 0.1$) and still obtain excellent converging results. In short, our experience shows that with reasonable initial estimates for the unknown parameters, the Marquardt method not only assures the convergence of iteration, it also results in the best fit in the least-squares sense that otherwise cannot be achieved either by the steepest descent method or by the Gauss method alone.

By looking at the shape of the magnetic anomaly curve, guided by the Werner total-field and horizontal-gradient solutions, and also with other available geophysical and geologic data, we should be able to provide adequate initial estimates from which we can apply Marquardt's algorithm. For a simple magnetic anomaly, we can use a four-corner body as our initial approximation. Even with this kind of simple anomaly, we have 11 unknown parameters to deal with; the x and z coordinates of each body corner ($2 \times 4 = 8$), magnetic susceptibility, mean value, and linear trend of the magnetic anomaly. The following three examples will illustrate the above procedure.

Example 1

In this example we demonstrate the applicability of Werner deconvolution and Marquardt modeling for determining depth to basement in petroleum exploration. Previously, the isolated anomaly shown in Figure 14 was interpreted to represent a basement source. From the cluster and spread of the Werner solutions, we can roughly outline the shape and boundary of the body as indicated by heavy lines. Using the Werner solutions as an initial estimate of the basement source, we applied Marquardt nonlinear least-squares best fit to a four-corner body. The residual error between observed and calculated total field indicated that a four-corner body was not sufficient to match the anomaly accurately, so we added extra corners to the model and repeated the Marquardt process after each addition. Finally, we obtained a six-corner body as a model of the source which gives an error between observed and calculated total field of less than 1 gamma. At each stage of our adjustment, less than five iterations were needed to obtain a best fit for a given number of corner points. By refining our initial Werner solutions, we were able to improve our basement estimate for this profile. Similarly, it would be possible to reinterpret entire basement surveys using Marquardt modeling to provide improved basement depth estimates, particularly if used in conjunction with gravity, seismic, and geologic information.

Example 2

In Figure 15 there are four magnetic anomalies along the line that correspond to four magnetic bodies. For ease of discussion we have numbered them 1 to 4 (left to right). On the basis of Werner deconvolution we interpreted the four anomalies to represent a massive body (body 1), a thin dike (body 2), an interface (body 3), and a smaller body (body 4). Again using the Werner solutions as our initial models, we carried out Marquardt refinement in four stages, each stage with a total of five iterations such that the final models showed residual errors of less than 1 gamma. Since body 2 is adjacent to the massive body 1 on its left and body 3 on its right, we encountered some difficulty in fitting that portion of the total field curve. Note that in our original interpretation body 3 was thought to represent a normal fault, but on the basis of Marquardt refinement it appears to represent a reverse fault instead. As in the previous example we were able to improve our original structural interpretation by using Marquardt modeling.

Example 3

Geothermal workers have suggested that it is possible to locate the Curie point isotherm by determining the depth to bottom of a magnetic body. This is a straightforward application of combined use of Werner deconvolution and Marquardt nonlinear least-squares best fit. As shown in the previous sections, an initial estimate of average rock susceptibility, shape, and depth to top are provided by Werner deconvolution of the observed magnetic field. We can use the Werner solution as starter models for further refinement by Marquardt modeling in which depth to bottom is determined by holding susceptibility and depth to top constant.

Synthetic magnetic anomalies resulting from three bodies were calculated by the method of Talwani and Heirtzler (1964) to simulate the Curie depth problem. We used these synthetic magnetic anomalies to test the Werner deconvolution and Marquardt modeling methods for their ability to resolve depth to bottom of magnetic structures. A synthetic profile runs from southwest to northeast (Figure 16a). Each model is assumed to be inductively magnetized in a geomagnetic field with an inclination of 59 degrees, declination of 14 degrees east, and an average field strength of 50,000 gammas.

We first subjected the synthetic magnetic anomalies to Werner deconvolution. Three Werner decimations were used in this analysis (3, 5, and 8 fiducials wide). Figure 16a shows the out-

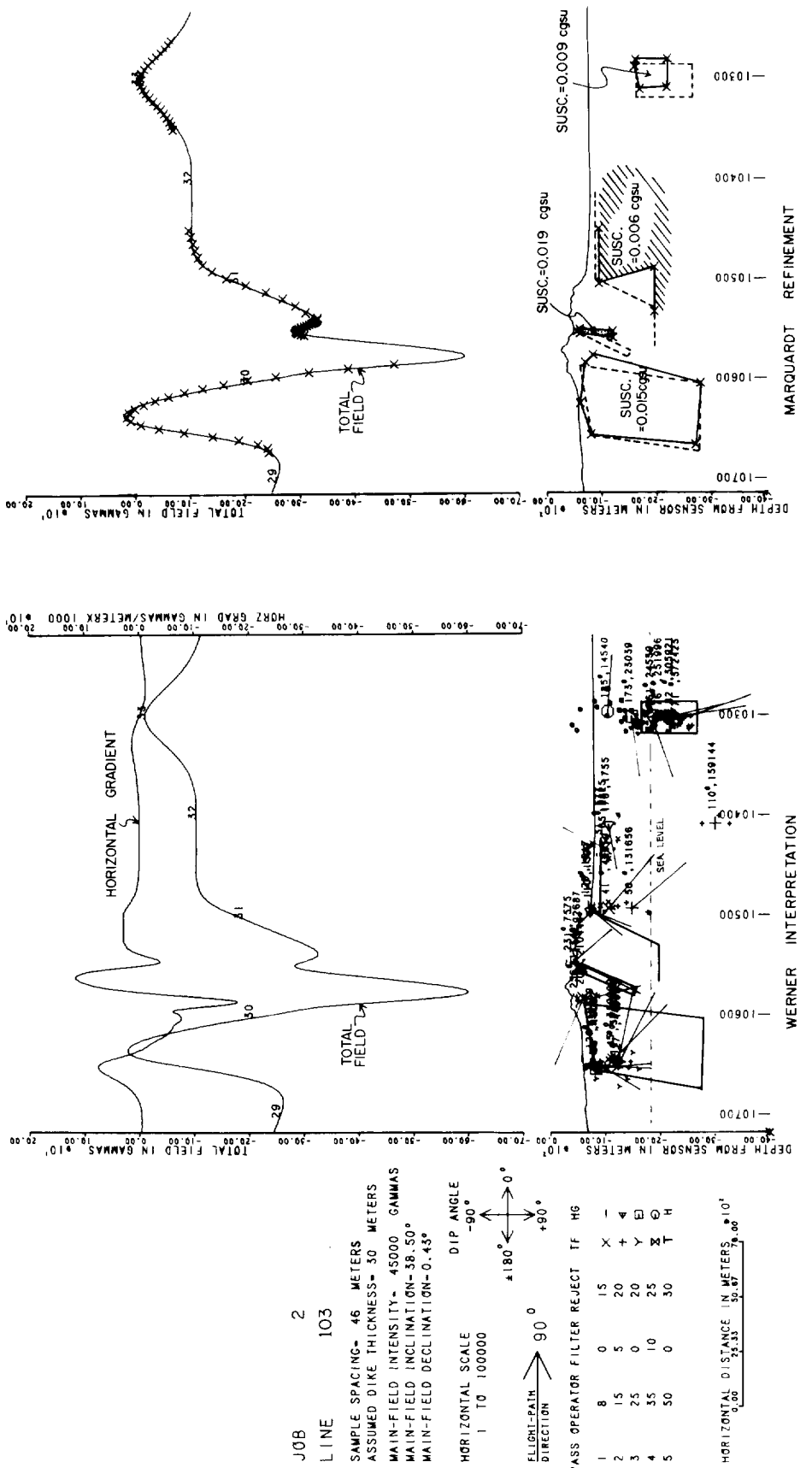

FIG. 15. Werner deconvolution and Marquardt refinement of four magnetic anomalies.

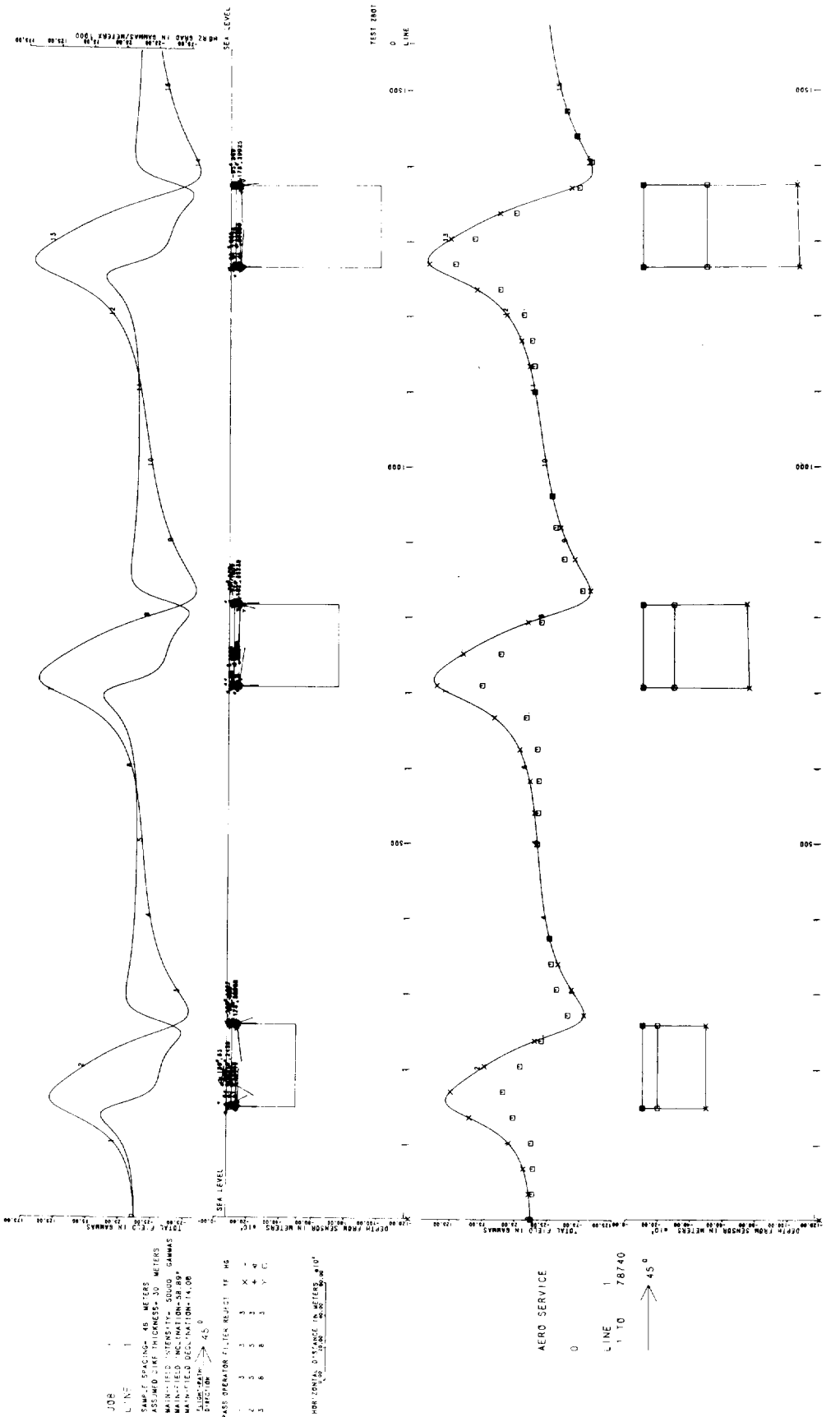

FIG. 16. (top) Werner deconvolution of synthetic magnetic anomalies caused by 3 model bodies. The horizontal gradient solutions define the depth, horizontal location, and susceptibility contrast of the sources. (bottom) Marquardt refinement of the initial starter models provided by the Werner analysis. Starter model is indicated by box symbols and the refined models by cross symbols.

line of the three models as well as the Werner solutions. Note that the depths estimated from the horizontal gradient are the correct choice for this example. Figure 16b shows the results of the Marquardt modeling. The corners of the initial starter models and the calculated total field values from the starter model are indicated by the large box symbols. We have displayed the final body coordinates and calculated total field data from the Marquardt adjusted models by large X's. After four iterations the computed depth to bottom values were all very close to the actual model values.

CONCLUDING REMARKS

We have presented a deconvolution for automated magnetic interpretation based on Werner's (1953) formulation of the thin-dike problem. The general utility of Werner deconvolution is extended by the fact that the horizontal gradient of the total field caused by the edge of a thick interface body is equivalent to the total field from the thin dike. Further, we have shown that iteration, statistical decision, and a seven-point Werner operator are necessary for valid estimates of the source body. Werner deconvolution essentially searches for variations in slopes and curvatures; thus it is able to recognize most anomalies and automatically compute their approximate horizontal location, depth, susceptibility contrast, and geometry.

One critical parameter involved in the Werner process that affects results of the deconvolution is selection of the Werner operator size. Choosing the correct parameters is presently an important step in the interpretation. By further study of the behavior of the Werner operator we should be able to automate the process fully to eliminate trial-and-error selection of parameters, thereby removing some of the existing uncertainty involved in using Werner deconvolution.

Once we have obtained the Werner solutions from analysis of the total field and horizontal gradient curves, we can conveniently use the solutions as initial estimates for further refinement by Marquardt nonlinear least-squares best fit modeling. We realize that the inversion is not unique in that different geometric models could equally fit the observed total field curves in the least-squares sense. Other geophysical and geologic information must be used to make the models realistic.

We have demonstrated the usefulness of Werner deconvolution on total field and horizontal gradient data. Extension of the method to vertical gradient data is a straightforward procedure. Since the vertical gradient is essentially high-pass filtering without phase shift, we can apply the Werner operator directly on the vertical gradient data, but the Werner vertical-gradient solution will be shallower in depth than the Werner total-field solution and in the same dip direction as the total-field solution.

ACKNOWLEDGMENTS

A portion of the work presented in this paper was performed while the authors were employed by Aero Service Division, Western Geophysical Co. of America. We thank Dr. E. J. Mateker, Jr. for company support and permission to publish the results.

We would like to express our sincere appreciation to Ron Hartman, President of International Exploration, Inc., for critically reading the manuscript and making many improvements. He also pointed out to the authors that Dr. H. Ackermann, formerly a geophysicist with Mobil, Sinclair, and Aero Service (now retired), was an important contributor to the application of Werner's writings for the computer. Thanks are also due Mr. Peter Brennan of Getty Oil and Glen Penfield of Aero Service for their constructive comments and encouragement.

REFERENCES

Hartman, R. R., Tesky, D. J., and Friedberg, J. L., 1971, A system for rapid digital aeromagnetic interpretation: Geophysics, v. 36, p. 891–918.

Hjelt, S. E., 1973, Experiences with automatic magnetic interpretation using the thick plate model: Geophys. Prosp., v. 21, p. 243–265.

Jain, S., 1976, An automatic method of direct interpretation of magnetic models: Geophysics, v. 41, p. 531.

Johnson, W. W., 1969, A least-squares method of interpreting magnetic anomalies caused by two-dimensional structures: Geophysics, v. 34, p. 65–74.

Ku, C. C., 1976, Numerical inverse magnetotelluric problems: Geophysics, v. 41, p. 276–286.

Marquardt, D. W., 1963, An algorithm for least-squares estimation of nonlinear parameters: J. Soc. Industr. Appl. Math., v. 11, p. 431.

McGrath, P. H., and Hood, P. J., 1973, An automatic least-squares multi-model method of magnetic interpretation: Geophysics, v. 38, p. 348–358.

Stanley, J. M., 1977, Simplified magnetic interpretation of the geologic contact and thin dike: Geophysics, v. 42, p. 1236–1240.

Talwani, M., and Heirtzler, J. R., 1964, Computation of magnetic anomalies caused by two-dimensional structures of arbitrary shape, *in* Computers in the mineral industries: G. A. Parks, Ed., Stanford Univ., p. 464–480.

Werner, S., 1953, Interpretation of magnetic anomalies at sheet-like bodies: Sveriges Geol. Undersok., Ser. C, Arsbok. 43 (1949), no. 6.

Wu, R. T., 1968, The inverse problem of magnetotelluric sounding: Geophysics, v. 33, p. 972–979.